Author version: *Boreas, vol.42(3); 2013; 762-778*

Record of carbonate preservation and Mid-Brunhes climatic shift from a seamount top with low sedimentation rates in the Central Indian Basin

BEJUGAM NAGENDER NATH, ADUKKAM V. SIJINKUMAR, DNYANDEV V. BOROLE, SHYAM M. GUPTA, LINA P. MERGULHAO, MARIA B. L. MASCARENHAS-PEREIRA, VENKITASUBRAMANI RAMASWAMY, MEDIMI V.S. GUPTHA, GÖRAN POSSNERT, ALA ALDAHAN, NANDKUMAR H. KHADGE AND RAHUL SHARMA

In the present investigation, age model of carbonate rich cores from a seamount top in the Central Indian Basin (CIB) was constructed using both isotopic ($^{230}Th_{excess}$, AMS ^{14}C, oxygen isotopes) and biostratigraphic methods. The chronologies using both the methods are in good agreement yielding a record of late Middle Pleistocene to Pleistocene-Holocene transition (550 to 11.5 ka). First appearance datum (FAD) of radiolarian *Buccinosphaera invaginata* (180 ka), coccolith *Emiliania huxleyi* (268 ka) and last appearance datum (LAD) of radiolaria *Stylatractus universus* (425 ka) were used. Monsoon-induced productivity increase was inferred from carbonate, organic carbon and $\delta^{13}C$ records responding to Mid-Brunhes Climatic Shift (MBCS), consistent with an increased global productivity. While the coccolith diversity increased, a decrease in coccolith productivity was found during MBCS. At nearly the same time period, earlier records from the equatorial Indian Ocean, western Indian Ocean and eastern Africa have shown an increased productivity in response to the influence of westerlies and increased monsoon. Influence of easterlies from Australia and the intensification of aridity are evidenced by increased kaolinite content and clay-sized sediments responding to the MBCS. Increased abundance of *Globorotalia menardii* and other resistant species beginning from marine isotope stage (MIS) 11 and proliferation of coccolith *Gephyrocapsa* spp. indicate increased dissolution which is consistent with the widespread global carbonate dissolution during this period. The relatively high carbonate dissolution during transition period of MIS 3/2 and glacial to interglacial period (MIS 6, 7 and 8) may be due to enhanced flow of corrosive Antarctic Bottom Water (AABW) into the CIB.

Bejugam Nagender Nath (e-mail: nagender@nio.org), Adukkam V. Sijinkumar (e-mail: sijingeo@gmail.com), Dnyandev V. Borole (e-mail: dnyanb@nio.org), Shyam M. Gupta (e-mail:smgupta@nio.org), Lina P. Mergulhao (e-mail: mlina@rediffmail.com), Maria B.L. Mascarenhas-Pereira (e-mail:mariab@nio.org), Venkitasubramani Ramaswamy (e-mail: rams@nio.org) and Medimi V.S. Guptha (e-mail: medimi.guptha@googlemail.com), Nandkumar H. Khadge (e-mail: khadge@nio.org) and Rahul Sharma (e-mail: rsharma@nio.org), Geological Oceanography Division, National Institute of Oceanography (CSIR), Dona Paula, Goa-403 004, India; Göran Possnert (e-mail: Goran.possnert@teknik.uu.se), Tandem Laboratory, Uppsala University, Uppsala, Sweden; Ala Aldahan[a,b], (e-mail: ala.aldahan@geo.uu.se), [a]Department of Earth Sciences, Uppsala University, Uppsala, Sweden, [b]Department of Geology, United Arab Emirates University, Al Ain, UAE.

***Present address**: A. V. Sijinkumar, Department of Post Graduate Studies & Research in Geology, Govt. College Kasaragod, Kerala, 671123, India; M.V.S. Guptha, 62, Sagar Society, Dona Paula, Goa, 403004, India.*

While the studies of past monsoon, upwelling and productivity prevailing in South and East Asia have received widespread attention, the palaeomonsoonal variation in areas south of southern limit of Intertropical Convergence Zone (ITCZ) in the Indian Ocean is poorly known. Central Indian Basin (CIB) provides such an opportunity, where it is expected that the summer monsoon can have greater effect than winter monsoon, due to weak and variable dry winds from the land towards the sea. Studies related to the reconstruction of monsoon and related productivity variations from CIB for the Quaternary are much fewer (e.g. Gupta 2003, 2009; Gupta *et al.* 2006) than north-western and north-eastern Indian Ocean. The Pleistocene palaeoceanographic changes of CIB have been studied by various workers based on micropalaeontological and geochemical variations (Pattan *et al.* 1992, 2005; Banakar *et al.* 1997, 2003; Gupta 1996; Gupta *et al.* 2006). Based on the distribution of modern monsoonal radiolarian assemblages (Gupta 1996) and their late Quaternary variations (Gupta & Fernandes 1997), Gupta *et al.* (1996) reconstructed tropical sea surface temperatures (SSTs) by the transfer function technique, and found the influence of earth's orbital eccentricity cycles on the monsoonal SSTs for the last ~1.4 Ma in the CIB.

Studies based on planktic foraminifera are lacking mainly due to non-availability of well preserved carbonate records. Since much of the sediments of the CIB are below CCD, carbonate dissolution limits their use for the reconstruction of palaeotemperature and palaeoceanographic conditions from foraminifera and their oxygen isotope analysis. Thus, the palaeoceanographic studies in the CIB so far have relied on radiolarian-based biostratigraphic and $^{230}Th_{excess}$ based radiometric dating methods (Banakar *et al*. 1991; Gupta 2002; Mascarenhas-Pereira *et al.* 2006; Nath *et al.* 2008). Here we present the first carbonate-based palaeoceanographic record from the CIB, which was possible due to sampling of seamount top, which is situated close to lysocline. We have studied the late Quaternary carbonate preservation and productivity changes based on planktic foraminifera, coccolithophores and geochemical proxies. We also show a record of regional response to Mid-Brunhes climatic shift (MBCS). The Mid Brunhes Event varies from 430 to 300 ka with amplitude of glacial-interglacial climate cycles increased substantially from early MIS 11 (Jansen *et al.* 1986). The chronological framework is constructed using radiolarian and coccolith biostratigraphy and radiochemical ($^{230}Th_{excess}$ and ^{14}C) methods, and finally the glacial-interglacial stages are identified using the oxygen isotope data.

Oceanographic settings

Studies of chemical properties of the water column in the CIB show three equator-ward moving water masses (de Sousa *et al*. 2001). The fastest moving water mass with subsurface salinity is

maximum in the depth range 125-200 m, characterized by high salinity (34.74-34.77 psu) and oxygen minimum associated with weak maxima in nutrients. The second water mass with deep oxygen maximum (234-245 µm) is in the depth range of 250-750 m, which is associated with minima in nutrients and relatively high pH. The third water mass present at depths 800-1200 m has a low salinity (34.71-34.72 psu) with a density (sigma-theta) range of 27.2-27.5 corresponds to the Antarctic Intermediate Water (AAIW) (de Sousa *et al.* 2001). The bottom is bathed by the North Indian Deep Water (NIDW) which is formed by mixing of Antarctic Bottom Water (AABW), North Atlantic Deep Water (NADW) and the deep water of the Northern Indian Ocean (Tchernia 1980). The abyssal depths (>4000 m) are filled with the water mass of the southern origin, mainly the AABW which is high in dissolved oxygen (Tchernia 1980; Warren 1982; Ramesh Babu *et al.* 2001). AABW is blocked by South East Indian Ridge on the southern side and Ninety East Ridge (except for the some openings) on the eastern side of the basin. The Central Indian Ridge acts as a barrier for the bottom water currents from the Madagascar and Crozet basins entering into this basin. According to Kolla *et al.* (1976) carbonate lysocline and carbonate critical depth (CCrD) along a latitudinal transect of 10°-20°S in the CIB are 4000 and 5050 m, respectively and further deepen towards south, whereas Banakar *et al.* (1998) placed the depth of lysocline at 4400 m and CCD at a depth of 4700m.

Materials and methods

Sampling

Two box cores BC 37 (16°06.031'S, 75°26.04'E, water depth: 4252 m, core length: 0.40 m) and SVBC 37 (16°06.943'S, 75°25.083'E, water depth: 3992 m, core length: 0.25 m) collected from the top of a seamount during 4th and 26th expeditions of R. V. Akademik Boris Petrov (Fig. 1) were used in the present study. The seamount from where the two sediment cores were collected is ~1200 m high rising from a seafloor depth of ~5100 m (Fig. 2). The seamount is located at the flanks of 76°30’E fracture zone (Fig. 2). The core BC 37 was sub- sampled at 2 cm intervals while SVBC 37 at 1 cm intervals for the present investigation. The core BC 37 was characterized by two distinct sediment layers, top 0-16 cm are foraminifera rich homogenous greyish orange pink sediments and bottom mixed layer of moderate brown to moderate yellowish brown sediments with dark yellowish orange intercalations whereas SVBC 37 is brown to white foraminiferal ooze. The location of cores from the seamount top provides us an opportunity to study the palaeoceanography of carbonate sediments in a predominantly siliceous ooze domain.

Foraminiferal analysis

About 10 g of dried samples were soaked in Milli-Q water overnight and washed through a 63 μm mesh sieve. Later the dried filtrate was sieved through 125 μm mesh sieve. The coarse fraction (>125 μm) was used for quantitative and qualitative analysis of planktic foraminifera assemblages under a stereo zoom binocular microscope. The same fraction was used for counting total benthic foraminifera. The samples were split into several aliquots to reduce the total number of planktic foraminifera to a minimum of 300 individuals. The taxonomic identification at species level is from Kennett & Srinivasan (1983). For radiolarian biostratigraphy, >63 μm fraction was used and late Quaternary radiolarian index microfossils are identified as described and illustrated in Gupta (1988) and employed for ascertaining the geological ages for the datum levels following Gupta *et al.* (1996). The ranking of different planktic foraminiferal species was based on their susceptibility to dissolution (based on a combination of rankings established by Bé (1977), Thunell & Honjo (1981) and Berger *et al.* (1982); (Table 1). Resistant species comprise of *Globorotalia menardii, Neogloboquadrina dutertrei, Pulleniatina obliquiloculata, Globorotalia tumida, Globorotalia crassaformis, Globorotalia truncatulinoides, Candeina nitida* and *Sphaeroidinella dehiscens.*

Determination of grain size and clay mineralogy

Salt free sediments were sieved to separate the less than 63 μm (silt and clay) fraction using deionised water (Milli-Q system). This silt and clay fraction was treated with 1:4 acetic acid to remove biogenic carbonate. Subsequently, the carbonate-free sediments were washed thoroughly with deionised water and centrifuged. The residue was further treated with 3% H_2O_2 to remove organic matter. After washing and centrifuging, 40 ml of Na_2CO_3 was added to dissolve biogenic silica/opal and transferred to 100 ml air tight plastic containers that were later kept in a water bath at a temperature of 90˚C for 5 hrs. The content from the containers was vigorously stirred at regular intervals of 1 hour. The suspension was later centrifuged and rinsed thrice with distilled water. The grain size distribution of the treated sediments which are now free from biogenic components were measured with a Malvern laser particle size analyzer (Mastersizer 2000) with a Hydro 2000 MU wet sampling accessory using procedures given in Ramaswamy & Rao (2006).

For clay mineral analysis, the clay fraction (<2 μm) was separated by settling technique according to Stokes law (Folk 1968) from the silt and clay lithogenic fraction. The salt and organic carbon-free sediment samples were prepared as thick slurry, pipetted onto glass slides, glycolated overnight at 60°C and kept in the desiccators. The clay slides were analyzed on a Philips X-ray

diffractometer using Ni-filtered Cu Kα radiation operated at 20 mA and 40 kV from 3° to 32° 2θ min^{-1}. The relative abundance of the clay minerals was determined according to the method described in Biscaye (1965) using weighted peak areas (4×illite, 2× kaolinite and chlorite) and (3.33×quartz).

AMS ^{14}C dating, oxygen isotope, $CaCO_3$ and organic carbon measurement

Approximately 10 to 16 tests of *Globigerinoides ruber* in the size range of 250-315 μm were used for oxygen isotope analysis. The shells were taken in thimbles, crushed by using thin needle, added a few drops of methanol and cleaned by using ultrasonic bath for 8-10 seconds. The cleaned tests were analysed using Isotope Ratio Mass Spectrometer at NIO, Goa. For AMS ^{14}C dating, nearly 5 mg of *G. menardii* were picked from 5 depth intervals and the dating was carried out at Uppsala University Tandem Accelerator facility, Sweden (BC 37) and Poznan Radiocarbon Laboratory, Poland (SVBC 37). Calendar age calibration was based on the CalPal 2007 programme (Weninger *et al.* 2007; http://www.calpal.de). Total carbon was determined using Carbon-Nitrogen elemental analyser and the carbonate carbon (TIC) was determined by Coulometer at NIO, Goa after acid evolution of CO_2. Organic carbon was estimated from the difference between total carbon and carbonate carbon. Mass accumulation rate (MAR) of $CaCO_3$ was calculated by using its concentration, linear sedimentation rate (LSR) and dry bulk density (DBD).

Coccolithophore studies

A small amount of sediment was suspended in water to which a few drops of hydrogen peroxide was added and kept overnight and ultrasonically treated to disaggregate the sediments. Then a drop of highly diluted solution was put on a glass slide, which was then dried using infra red light and coated with (Gold-Palladium) at 100 Å in a sputter coater. This gold-coated sample stub was scanned using JSM-5800 LV SEM at 15 KV. Species composition and abundances were determined by identifying and counting the species of coccolith randomly at a magnification of x 3500 for 20 fields of view. Identification of various taxa of coccolithophorids was done following the references of Winter *et al.* (1994) & Kleijne (1993). Diversity was expressed as the Shannon's Index (H′), measuring a combination of species richness and evenness of distribution on specimens over species and was carried out using the Primer Software (Clarke & Gorley 2001).

Radiochemical analyses

Radiochemical analyses were carried out on samples taken at 2 cm intervals within the core. About 1-2 g dried sediments were brought into solution by HF-$HClO_4$-HNO_3-HCl digestion in the presence

of ^{208}Po and ^{232}U/^{228}Th spike and therefore represent bulk analyses. The ^{210}Pb was measured via its daughter nuclide ^{210}Po, using the standard radiochemical procedures after auto deposition (for details see Flynn 1968 and Anderson & Fleer 1982). After the auto deposition of Po, the solution was dried and the residue was digested with HNO_3 and dissolved in 9 M HCl. U-Th radiochemical separations and purification were carried out following the standard procedure of Krishnaswami & Sarin (1976). The alpha activity of the electroplated sample was assayed using ion implanted detector coupled to Octete plus Alpha spectrometer (EG & G ORTEC). The values for $^{230}Th_{excess}$ were calculated by subtracting the ^{234}U activity from the total ^{230}Th activities.

Results

Biostratigraphy, $^{230}Th_{excess}$, AMS ^{14}C, oxygen and carbon isotope

The age models for the cores are based on multiple dating techniques. While we used dating tools such as $^{230}Th_{excess}$, AMS ^{14}C, oxygen isotope and biostratigraphy (radiolarian and coccolith) for establishing the age model for the core BC 37 (Table 2, Fig. 3A, B), the age model for SVBC 37 is constructed mainly using biostratigraphy, AMS ^{14}C and the correlation with nearby BC 37 (Table 3, Fig. 3B). The first appearance of *Buccinosphaera invaginata* (180 ka) is seen at 4-6 cm interval (5-6 cm in SVBC 37) and the last appearance of *Stylatractus universus* (425 ka) at 32-34 cm (20-21 cm in SVBC 37). In core SVBC 37, the younger age marker of the radiolaria (*B. invaginata*) and *Emiliania huxleyi* is used for the final age model. *E. huxleyi,* age-diagnostic nannofossil occurs from the top section (0-2 cm) to a depth of 18-20 cm in core BC 37 and 18-19 cm in SVBC 37 (Fig. 3A, B; Tables 2, 3), representing the age of first occurrence.

The decay curve of $^{230}Th_{excess}$ for sediment section between 0 cm and 26 cm is linear with depth (Fig. 3C) and the estimated sedimentation rate is 0.62 mm ka^{-1} and corresponds to an age of ~420 ka for the sediments at 26 cm (this estimate is close to the dating limit of $^{230}Th_{excess}$ method, half life = ~75 ka). Although the $^{230}Th_{excess}$ values in sediments deeper than 26 cm are not exactly linear, we have extrapolated the sedimentation rate to assign an age for the base of the core. Five sediment sections from both cores were used for AMS ^{14}C dating. Among them, only the surface sections (0-2 cm) have given an age of 13.82±163 cal. ka BP for core BC 37 (Table 2), and 12.83±86 cal. ka BP for SVBC 37 (Table 3) whereas, the deeper sections (2-3, 20-22 and 38-40 cm) are beyond the dating limit of radiocarbon and hence represent an age older than ~45 ka (Tables 2, 3). The *G. ruber* oxygen isotope stratigraphy of core BC 37 was plotted and found to have a continuous record since MIS 14 (Fig. 4A). Very low sedimentation rates preclude sample representation from

MIS 1 and lead to fewer sample points in other stages, and limit the formation of smooth oxygen isotope curve (Fig. 4A). However, glacial to interglacial boundaries identified from oxygen isotope data also match with the chronology developed by other methods (Table 2). The $\delta^{13}C$ values for BC 37 show positive and high values in latest Pleistocene (~300 to 14 ka) and low values between 550 and 300 ka (Fig. 4B; Table 4).

Organic carbon, $CaCO_3$, grain size and clay mineralogy

The C_{org} content is significantly low in both cores and it is ranging from below detection to 0.21% (Table 4). Relatively higher C_{org} values are observed during the last 300 ka compared to the low values during 300 to 550 ka (Fig. 4C, F). $CaCO_3$ content in SVBC 37 is higher than BC 37 and the values range between 77 and 92% and 48 and 78%, respectively (Table 4; Fig. 4D, E). Variations in the $CaCO_3$ and C_{org} values follow each other and both show higher values during the last 300 ka (Fig. 4). MAR of $CaCO_3$ for both cores is similar to the downcore variation of $CaCO_3$% (Fig. 4D-G). The record of downcore variation of clay minerals (kaolinite + chlorite %) and grain size class (<2 μm and 8-16 μm) are shown in Fig. 5. A distinct increase in the kaolinite% along with chlorite% is noticed at about 270 ka (Fig. 5A). At the termination of MIS 11, another distinct increase in the clay-sized lithogenic material (<2 μm) is concomitant with a decreasing trend of coarser fine silt (8-16 μm; Fig. 5B, C).

Coccolithophore record and ranking of planktic foraminiferal dissolution indices

The downcore variation of *Gephyrocapsa oceanica*, *Gephyrocapsa caribbeanica*, *Gephyrocapsa* spp. and *E. huxleyi* along with Shannon-Wiener Diversity Index of coccolithophores is shown in Fig. 6A-E. *Gephyrocapsa* spp. shows a major increase from MIS 14 to 8 whereas Shannon-Wiener Diversity Index of coccolithophores shows a conspicuous decrease during global Mid-Brunhes Dissolution Interval (MBDI). A sudden increase in diversity of cocolithophores is seen at 300 ka onwards. Planktic foraminiferal assemblages of both the sediment cores yielded 23 species with *G. menardii* constituting the most abundant species in both the cores (Figs. 7H, 8A; Table 1). Furthermore, differences in foraminiferal assemblages are very conspicuous which is reflected in their susceptibility to dissolution (Figs. 7A-F, 8A-G). Based on the ranking scheme of species prone to dissolution employed here (by combining the schemes proposed by Bè 1977, Thunell & Honjo 1981 and Berger *et al.* 1982 of planktic foraminifera), we find that about 60% in core SVBC 37 (3992 m) and about 80% in BC 37 (4252 m) are resistant species (Table 1).

Discussion

Chronology

The carbonate sediments of our samples provided an opportunity to date the sediments by several methods. The biostratigraphy used in this work is based on the Quaternary index fossils of radiolaria and coccolithophore (mainly *E. huxleyi).* The radiolarian index events were calibrated to an "absolute" time scale based on the palaeomagnetic polarity time scale by Johnson *et al.* (1989). Two synchronous radiolarian biostratigraphic datum levels such as first appearance datum (FAD) of *B. invaginata* (~180 ka) and last appearance datum (LAD) of *S. universus* (~425 ka) were used (Johnson *et al*. 1989; Gupta 2002) (Fig. 3A). These two synchronous radiolarian biostratigraphic datum levels were widely used in reconstructing chronology of the late Quaternary sediments of the CIB (Gupta 1988, 2002, 2003; Nath *et al.* 2008). *B. invaginata* is the index species of the very first and topmost zone of the Neogene radiolarian biostratigraphy. The accuracy of the age model based on the two biostratigraphic events in a sediment section from the equatorial Indian Ocean was found to be ±2 ka at tilt and ±1 ka at precession bands (4% error) (Gupta 2002). *Collosphaera tuberosa* (FAD 650 ka) is present throughout the core BC 37 suggesting that the cored sediment section is not older than 650 ka (Gupta 2002) (Table 2). The nannofossil index fossil such as FAD of *E. huxleyi* is commonly used to assign the age of 268 ka BP. This corresponds closely to the ages (306 and 302 ka respectively) estimated for the same depth using $^{230}Th_{excess}$ and radiolarian index fossils chronology (Table 2). The FAD of *E. huxleyi* is synchronous worldwide in the tropical to subtropical region of the open ocean (Thierstein *et al.* 1977). Depending on the different proxies used and the location, FAD of *E. huxleyi* has been dated at ~270000 years using correlation with planktic foraminiferal $\delta^{18}O$ records (Gartner & Emiliani 1976) and at ~268000 years ago in oxygen isotopic stage 8 (Thierstein *et al.* 1977).

The $^{230}Th_{excess}$ based sedimentation rate of 0.62 mm ka^{-1} is comparable to 0.72 mm ka^{-1} derived from coccolith and radiolarian-based biostratigraphy (Fig. 3C). Similar record of low sedimentation rate (0.32 mm ka^{-1}) was also reported on the flank of same seamount in CIB (Mascarenhas-Pereira *et al.* 2006) and such a low sedimentation rate (see Banakar *et al.* 1991; Borole 1993; Gupta *et al*. 1996) limits the extraction of high resolution variability from these records. Sediments of core BC 37 record a longer age span (550 to 14 ka) compared to SVBC 37 which extends to MIS 10 (355 to 13 ka). Thus, these carbonate sediment cores provided us with an opportunity to correlate various dating tools to reconstruct the late Quaternary (late Middle Pleistocene to Pleistocene-Holocene transition) palaeoceanographic record in the CIB.

Increased productivity at Mid-Brunhes Epoch

Oxygen and carbon isotope record shows a long term characteristic change from 300 ka onwards (Fig. 4A, B; Table 4) with a concomitant change also noticed in other productivity proxies of C_{org}, $CaCO_3$, total benthic foraminifera (TBF) and total planktic foraminifera (TPF) (Table 4; Fig. 4C-J) marking a response to the MBCS. This climate shift has been correlated with the so called 'Mid-Brunhes climate event' centred on 300 ka that has been recorded in many proxies (Kershaw *et al.* 2005 and references therein). The high abundance peaks of C_{org}, $CaCO_3$ and $\delta^{13}C$ and increased MAR of $CaCO_3$ coincide with high abundance of TPF and total benthic foraminifera TBF suggesting an increase in surface and bottom water productivity during the last 300 ka (Fig. 4). Increased carbonate accumulation at MBCS shown in sediment record is consistent with the global increase in carbonate productivity (Barker *et al.* 2006 and references therein). A broad maximum in $CaCO_3$ accumulation is seen in the East Equatorial Pacific during the Mid-Brunhes interval (Snoeckx & Rea 1994). Increased global $CaCO_3$ accumulation at MBCS has been attributed by Barker *et al*. (2006) to an increase in surface ocean carbonate production.

Similar MBCS related influence is also manifested by a distinct increase in the radiolarian (Rads g^{-1}) in a sediment record located at 7°48' S (about ~500 miles north of our record) in the CIB (Gupta 2009) at about ~250 ka BP (exactly conformable with our sediment record) implying an increase in monsoon-driven productivity (Fig. 5H). Increased amplitudes of high frequency (sub-orbital) 17, 15, and 13 ka cycles were also evident at MBCS (Gupta 2009). Later, Gupta *et al.* (2010) also interpreted the abrupt decrease in *Globigerina bulloides* population at MBCS across MIS 9 and 8 (~300-250 ka) at Hole 716A (04°56'N; 73°17'E) in the equatorial Indian Ocean as a major decrease in Indian Ocean equatorial westerlies (IEW) strength and increase (positive mode) in Indian Ocean Dipole (IOD) strength. This behaviour may relate to consequent climate change in the surrounding equatorial regions including East Africa and Australasia (Fig. 5G). Gupta *et al.* (2010) have further argued that the IEW remained weak following the Mid-Brunhes transition with significantly reduced variability, suggesting an overall strengthened (positive) IOD. Incidentally, vegetation changes were witnessed in the regions east and west of the Indian Ocean with Australasia experiencing wet conditions prior to the transition (~460 to ~300 ka) (Fig. 5G) (Kawamura *et al.* 2006) whereas tropical Africa experienced dry conditions (Jansen *et al.* 1986) suggesting a strengthened IEW and negative IOD condition. In contrast, our sediment record which is further south (20° south of Hole 716 which is about 1200 nautical miles) shows a distinct increase in productivity during Mid-Brunhes epoch and corresponds to an increased productivity in the NW

Arabian Sea at the same time period (Hole 723B; Emeis *et al.* 1995 and Hole 728B; Gupta *et al.* 2010). Thus, the Mid-Brunhes shift in productivity south of equator (our data) is more likely due to strengthening of easterlies, as such event coincides with a shift towards dry conditions in Australasia (Kershaw *et al.* 2005 as quoted in Gupta *et al.* 2010). Low precipitation conditions in the eastern Indian Ocean are also evidenced by an increase in grassland taxa after 300 ka in Timor Sea (Kawamura *et al.* 2006). At the same time, equatorial East Africa turned wetter (Jansen *et al.* 1986) and the Indian summer monsoon intensified (Emeis *et al.* 1995).

High abundance of coccolithophore *E. huxleyi* and low abundance of *Gephyrocapsa* spp. are observed from 300 ka onwards with increased Shannon-Wiener Diversity Index (H') of coccolithophores marking the response to MBCS (Fig. 6A-E) which is concomitant to the increases in C_{org} and $CaCO_3$ at about the same time. Such a change could reflect either an absolute increase in primary productivity or an increase in the efficiency of C_{org} export from the surface ocean (Barker *et al.* 2006). The ballast hypothesis suggests that $CaCO_3$ may be the most important agent for transporting organic carbon to the deep sea, representing up to 83% of the flux of C_{org} in certain environments (Armstrong *et al.* 2002; Barker *et al.* 2006). Export of C_{org} may strengthen the organic pump and help in drawdown of CO_2 in the surface ocean, balancing the CO_2 rise from the increased production of $CaCO_3$ in the surface ocean (Barker *et al.* 2006). A distinct peak of $\delta^{13}C$ is noticed during MIS 11 in our record which is consistent with the global maximum in $\delta^{13}C$ during this period (Wang *et al.* 2004; Barker *et al.* 2006). Relatively heavier $\delta^{13}C$ values at MBCS however correspond with that of $CaCO_3$ and C_{org} (Fig. 5B-F) which is contemporaneous with increased global carbonate dissolution (Barker *et al.* 2006). Organic carbon is also relatively low during 300 to 550 ka indicating a well-oxygenated bottom water environment and low productivity in contrast to the relatively high C_{org} during the last 300 ka.

Inferring Mid-Brunhes change in wind regime and increased aridity in Australian region

A distinct increase in the kaolinite% along with chlorite% is noticed at about 270 ka which coincides with the influence of Mid-Brunhes climatic change (Fig. 5A). At the termination of MIS 11, another distinct increase in the clay-sized lithogenic material (<2 μm) is concomitant with a decreasing trend of coarser fine silt (8-16 μm; Fig. 5B, C). Increased clay size together with a concomitant increase in kaolinite% suggests high supply of kaolinite-rich dust to the CIB. Kaolinite is the dominant mineral of western Australia (in the eastern Indian Ocean) the source of which has been attributed to wind transport (Griffin *et al.* 1968; Fagel 2007). Griffin *et al.* (1968) and Kolla & Biscaye (1973) show a tongue of kaolinite-rich sediment extending westward from the Northwest Cape into the Indian

Ocean (Fig. 1) and our study area juxtaposes the kaolinite-rich region off Australia (Fig. 1). Kaolinite-rich dust is blown into the eastern Indian Ocean due to the prevailing easterly winds and may increase the overall kaolinite content of the pelagic sediments (McTainsh 1989; Gingele *et al.* 2001). Gingele *et al.* (2001) found kaolinite and illite to be the dominant major minerals both in the dust samples and the marine samples. Increased dust at the Mid-Brunhes epoch in our sediment record suggests an intensification of aridity in Australia and dust transport to our site in the middle of the Indian Ocean. This interpretation is consistent with the onset of dry conditions in Australasia at about this time period (Kershaw *et al.* 2005; Gupta *et al*. 2010) where the earliest arid landforms date from at least 300 ka (Bowler 1976). Gupta *et al.* (2010) has related Mid-Brunhes monsoon intensification in the western Indian Ocean and also the eastern Africa to the influence of Indian Ocean Dipole (IOD) event. Clear manifestation of Mid-Brunhes productivity in our sediment record may also confirm intensification of IOD related monsoon. Monsoon intensification following an increased aridity in the eastern Indian Ocean is also a feature of the IOD (Abram *et al.* 2007). Early phase of IOD drought corresponds with the Asian summer monsoon season (~May-September) and is probably caused by strengthened cross-equatorial airflow drawing moisture from the tropical Indian Ocean into the Asian monsoon (Abram *et al*. 2007). Similar process must be responsible for increased monsoon, during Mid-Brunhes period; as our study area is located exactly half-way between the areas influenced by IOD.

Intra- and inter-core carbonate preservation patterns: Dissolution related to lysoclinal depth and the glacial-interglacial climatic changes

In the present investigation, carbonate dissolution is encountered as evidenced by the presence of corroded planktic foraminiferal specimens and broken keels of *G. menardii* implying that the cores under investigations are retrieved from close to lysocline. Based on the ranking of planktic foraminifera susceptible to dissolution, we find that about 60% (SVBC 37; 3992 m) to 80% (BC 37, 4252 m) of foraminifers are resistant (Table 1), reflecting the degree of dissolution intensity in these two cores. Higher $CaCO_3$ content (77 to 92%) in SVBC 37 over core BC 37 (and 48 to 75%; Table 4) also supports the foraminifera-based interpretation. This has resulted in low foraminiferal diversity and abundance of resistant planktic foraminifera. While the number of foraminiferal assemblages present in both cores is the same, shallow core SVBC 37 shows better preservation of foraminifera. The high abundance of resistant species in both cores however may suggest some degree of supralysoclinal dissolution. The relative abundance of most susceptible species *G. ruber* (Rank 1) is very low (8^{th} most abundant species) in core BC 37 whereas significantly high (2^{nd} most

abundant species) in SVBC 37 (Table 1). The significant dissolution in core BC 37 (water depth ~4250 m) relative to SVBC 37 (water depth ~3990 m) provides indications of placing the foraminiferal lysocline shallower (approximately at a depth of 4250 m) than the earlier estimate of 4400 m in CIB (Banakar *et al*. 1998). While the overall difference in $CaCO_3$ content and foraminiferal assemblages between the two cores are related to the lysocline depth, significant dissolution events within each core are seen during transitional period between MIS 3/2 and glacial interglacial periods such as MIS 6, 7 and 8 (Figs 7, 8) which could reflect the response to past oceanographic/climatic conditions.

In the Pacific Ocean, late Quaternary dissolution maxima was found to correlate with the deglacial periods and the minima with transitional periods from interglacial to glacial conditions (Wu *et al.* 1991; Murray *et al.* 2000). According to Sexton & Barker (2012), the $CaCO_3$ content of deep-sea sediments in the Pacific Ocean increases during glacials of the Late Pleistocene in comparison to interglacials, whereas records of sedimentary $CaCO_3$ in the Atlantic Ocean show an anticorrelated pattern across glacial-interglacial cycles; this pattern however existing since ~1.10 Ma only. Before this, both patterns in both oceans were in-phase, and had 'Atlantic-style' phasing with respect to glacial–interglacial cycles; the change in Pacific $CaCO_3$ dissolution cyclicity at 1.10 Ma caused by switching over of the relative ventilation state of abyssal South Pacific waters between glacials and interglacials (Sexton & Barker 2012). Different views exist on the control of carbonate preservation in the Pacific, either in favour of productivity (e.g. Murray *et al.* 2000) or solely in favour of dissolution control (e.g. Anderson *et al.* 2008). Past corrosion of pelagic $CaCO_3$ in the central equatorial Pacific was not found to covary with the observed sedimentary concentration of $CaCO_3$ (LaMontagne *et al.* 1996) suggesting a decoupling between $CaCO_3$ content and carbonate dissolution indices which is also seen in our records from the CIB (Figs 7, 8).

Increased abundance of dissolution resistant species *G. menardii, G. menardii* fragments, dissolution index (ratio of non-resistant to resistant species) and other resistant species starting from MIS 11 (until MIS 7) suggests selective dissolution process during this period which is consistent with other global records (Barker *et al.* 2006). Being a period of global carbonate dissolution, MIS 11 is also marked by increased $CaCO_3$ accumulation in a variety of locations (Barker *et al.* 2006). Our coccolithophore record from CIB shows a major increase of *Gephyrocapsa* spp. during MIS 14-8 which is well matching with earlier records (Bollmann *et al*. 1998; Barker *et al.* 2006). According to Barker *et al.* (2006), global increase in pelagic carbonate production, possibly associated with the proliferation of the *Gephyrocapsa* spp., has caused widespread dissolution during Mid-Brunhes.

Shannon-Wiener Diversity Index of coccolithophores shows a conspicuous decrease during MBDI and sudden increase in diversity at 300 ka onwards marking response to MBCS. MBDI represents a major perturbation to the global ocean carbon system (see Barker *et al.* 2006). Flores *et al.* (2003) noted the correspondence between high $CaCO_3$ and the increased abundance of *Gephyrocapsa*, contemporaneous with enhanced dissolution during the Mid-Brunhes in ODP site 1089. The high carbonate dissolution episodes during transition period of MIS 3/2 and interglacial period (MIS 7) and glacial period (MIS 6 and 8) may be due to the enhanced flow of corrosive AABW or increased productivity during Late Pleistocene. CIB is bathed by AABW which is considered to be significantly corrosive and can induce sediment erosion recorded in cores from CIB (Banakar *et al.* 1991). AABW crosses the south eastern Indian Ridge and flows to western margins of the South Australian Basin and Wharton Basin and continues northwards along the base of the Ninety-East Ridge and enters the CIB (Johnson & Nigrini 1982). It causes dissolution of biogenic silica which is seen in enhanced values of interstitial silica content (Nath & Mudholkar 1989). AABW production has occurred during both glacial and interglacial periods and has shown changes in circulation for the last 500 ka (Corliss 1979). Incidentally, the time periods during which we find intense dissolution in our sediment record and high abundance of diatoms (during the MIS 6/7 and MIS 3/2 boundaries) are correlated with two periods of maximum AABW flow during the last 240 ka (Jones & Johnson 1984).

Conclusions

The chronology of carbonate sediments from a seamount in the Central Indian Basin was established by using fossil markers (radiolarian and coccoliths), $^{230}Th_{excess}$, and AMS ^{14}C which has provided a sedimentary record of late middle Pleistocene to Pleistocene-Holocene transition (550 to 11.5 ka). While all the early records of paleoceanographic interpretations from the Central Indian Basin were based on radiolarian stratigraphy and $^{230}Th_{excess}$ methods, carbonate sediment cores provided us with an opportunity to correlate various dating tools. The sedimentation rates derived from $^{230}Th_{excess}$ method were ~0.62 mm ka^{-1} was in good agreement with a sedimentation rate of 0.72 mm ka^{-1} yielded from biostratigraphic datum levels. From the chronology established, the following palaeoclimatic inferences are drawn:

- These Late Pleistocene carbonate records from the CIB show that the monsoon induced productivity has increased from ~300 ka displaying a distinct response of monsoon to Mid-Brunhes climatic shift with increasing trend at the end of MIS 11. Increased Mid-Brunhes productivity in our record is consistent with a global increase in carbonate productivity. Influence

of MBCS was also reflected from coccolith records where a distinct change in the species diversity was noticed.

- Concomitant changes were also noticed in the wind proxies such as mean particle size and clay mineral content. Increased clay-sized material (<2 μm) and kaolinite content at the same time (Mid-Brunhes) indicates the intensification of easterlies from Australia.

- Manifestation of Mid-Brunhes productivity in our sediment record may suggest the intensification of Indian Ocean Dipole (IOD) related monsoon, similar to the earlier reports of IOD-driven Mid-Brunhes monsoon intensification in the northwestern Indian Ocean and the eastern Africa.

- Total resistant species, ratio of non-resistant to resistant species and *G. menardii* fragments clearly shows the intensity of carbonate dissolution varied with glacial-interglacial cycles and dissolution is very high in core BC 37 from deeper depth (4252 m) than the shallower core SVBC 37 (depth 3992 m) suggesting that the lysocline could be shallower than the previous estimate for CIB.

- Increased abundance of *G. menardii* and its fragments beginning from MIS 11 and proliferation of coccolith *Gephyrocapsa* spp. are indicating dissolution which is consistent with the widespread global carbonate dissolution during this period. High carbonate dissolution during transition period of MIS 3/2 and glacial to interglacial period (MIS 6, 7 & 8) may be due to enhanced flow of corrosive AABW into the CIB.

Acknowledgements. -We thank the Director of the National Institute of Oceanography, Goa, for the permission to publish this paper. Ministry of Earth Science (formerly Department of Ocean Development, Govt. of India) New Delhi is thanked for providing ship time of Akademik Boris Petrov and funding for Project PMN-EIA. Captain and crew of the ship are also thanked for their help. Ms. Trupti Naik helped in shipboard sampling and sample processing in shore lab. M/s V.D. Khedekar, Girish Prabhu, Ms. Supriya Karapurkar and Dr. C. Prakash Babu are thanked for their help during SEM, XRD, IRMS and Coulometer analyses respectively. Sediment grain size and mineralogy were generated as a part of Graduate project work of students of Smt. Parvatibai Chowgule College, Margao. Comments by Dr. Richard Murray and the anonymous reviewer and changes suggested by Prof. Jan Piotrowski, Editor-in-Chief have helped in improving the manuscript. This is National Institute of Oceanography contribution No._____.

References

Abram, N. J., Gagan, M. K., Liu, Z., Hantoro, W. S., McCulloch, M. T. & Suwargadi, B. W. 2007: Seasonal characteristics of the Indian Ocean Dipole during the Holocene epoch. *Nature 445*, 299-302.

Anderson, R. F. & Fleer, A. P. 1982: Determination of natural actinides and plutonium in marine particulate material. *Analytical Chemistry 54*, 1142-1147.

Anderson, R. F., Fleisher, M. Q., Lao, Y. & Winckler, G. 2008: Modern $CaCO_3$ preservation in equatorial Pacific sediments in the context of late-Pleistocene glacial cycles. *Marine Chemistry 111,* 30-46.

Armstrong, R. A., Lee, C., Hedges, J. I., Honjo, S. & Wakeham, S. G. 2002: A new, mechanistic model for organic carbon fluxes in the ocean based on the quantitative association of POC with ballast minerals. *Deep-Sea Research II 49*, 219-236.

Banakar, V. K., Gupta, S. M. & Padmavathi, V. K. 1991: Abyssal sediment erosion in the Central Indian Basin: Evidence from radiochemical and radiolarian studies. *Marine Geology 96*, 167-173.

Banakar, V. K., Pattan, J. N. & Mudholkar, A. V. 1997: Palaeoceanographic conditions during the formation of a ferromanganese crust from the Afanasiy-Nikitin seamount, North Central Indian Ocean: geochemical evidence. *Marine Geology 136*, 299-315.

Banakar, V. K., Parthiban, G., Pattan, J. N. & Jauhari, P. 1998: Chemistry of surface sediment along a north-south transect across the equator in the Central Indian Basin: assessment of biogenic and detrital influences on elemental burial on the seafloor. *Chemical Geology 147*, 217-232.

Banakar, V. K., Galy, A., Sukumaran, N. P., Parthiban, G. & Volvaikar, A. Y. 2003: Himalayan sedimentary pulses recorded by silicate detritus within a ferromanganese Crust from Central Indian Ocean. *Earth & Planetary Science Letters 205*, 337-348.

Barker, S., Archer, D., Booth, L., Elderfield, H., Henderiks, J. & Rickaby, R. E. M. 2006: Globally increased pelagic carbonate production during the Mid-Brunhes dissolution interval and the CO_2 paradox of MIS 11. *Quaternary Science Reviews 25,* 3278-3293.

Bé, A. W. H. 1977: An ecological zoogeographic and taxonomic review of recent planktonic foraminifera. *In* Ramsey, A. T. S. (ed.): *Oceanic Micropaleontology, 1-88. Academic Press, London.*

Berger, W. H., Bonneau, M. –C. & Parker, F. L. 1982: Foraminifera on the deep-sea floor: lysocline and dissolution rate. *Oceanologica Acta 5*, 249-258.

Biscaye, P. E. 1965: Mineralogy and sedimentation of recent deep-sea clay in the Atlantic Ocean and adjacent seas and oceans. *Geological Society of America Bulletin 76*, 803-831.

Bollmann, J., Baumann, K. H. & Thierstein, H. R. 1998: Global dominance of Gephyrocapsa coccoliths in the late Pleistocene: selective dissolution, evolution, or global environmental change? *Paleoceanography 13,* 517-529.

Borole, D. N. 1993: Late Pleistocene sedimentation: A case study of the Central Indian Ocean Basin. *Deep-Sea Research (A: Oceanographic Research Papers) 40,* 761-775.

Bowler, J. M. 1976: Aridity in Australia: Age, origins and expressions in Aeolian landforms and sediments. *Earth Science Reviews 12*, 279-310.

Clarke, K. R. & Gorley, R. N. 2001: Primer V5: User M/Tutorial, PRIMER-E. Plymoth, U.K.

Corliss, B. H. 1979: Quaternary Antarctic bottom water history: Deep sea benthonic foraminiferal evidence from the south East Indian Ocean. *Quaternary Research 12*, 271-289.

de Sousa, S. N, Sardessai, S. D., Ramesh Babu, V., Murty, V. S. N. & Gupta, G. V. M. 2001: Chemical characteristics of Central Indian Basin waters during the southern summer. *Deep-Sea Research II 48*, 3343-3352.

Emeis, K. C., Anderson, D. M., Doose, H., Kroon, D., Schulz, D. & Schulz-Bull, D. 1995: Sea-surface temperatures and the history of monsoon upwelling in the northwest Arabian Sea during the last 500,000 years. *Quaternary Research 43*, 355-361.

Fagel, N. 2007: Marine clay minerals, deep circulation and climate. *In* Hillaire-Marcel, C. & de Vernal, A. (eds.): *Proxies in Late Cenozoic Paleoceanography,* p.139-184. Elsevier, Amsterdam

Flores, J. A., Marino, M., Sierro, F. J., Hodell, D. A. & Charles, C. D. 2003: Calcareous plankton dissolution pattern and coccolithophore assemblages during the last 600 kyr at ODP Site 1089 (Cape Basin, South Atlantic): palaeoceanographic implications. *Paleogeography, Paleoclimatology, Paleoecology 196*, 409-426.

Flynn, W. W. 1968: The determination of low levels of polonium-210 in environmental samples. *Analytica Chimica Acta 43*, 221-227.

Folk, R. L. 1968: *Petrology of Sedimentary Rocks*. 170 pp. Hemphill, Austin.

Gartner, A. & Emiliani, C. 1976: Nannofossil biostratigraphy and climate stages of Pleistocene Brunhes Epoch. *American Association of Petroleum Geologists Bulletin 70,* 1562-1564.

Gingele, F. X., Deckker, P. D. & Hillenbrand, C. D. 2001: Clay mineral distribution in surface sediments between Indonesia and NW Australia-Source and transport by ocean currents. *Marine Geology 179*, 135-146.

Gordon, A.L., Claudia, F., Giulivi, T.T., Stewart, S., John, M., and Donald, O. 2002, Bay of Bengal nutrient-rich benthic layer: *Deep-Sea Research II 49*, 1411–1421.

Griffin, J. J., Windom, H. L. & Goldberg, E. D. 1968: The distribution of clay minerals in the world ocean. *Deep-Sea Research 15*, 433-459.

Gupta, A. K., Das, M. & Bhaskar, K. 2006: South Equatorial Current (SEC) driven changes at DSDP Site 237, Central Indian Ocean, during the Plio-Pleistocene: evidence from benthic foraminifera and stable isotopes. *Journal of Asian Earth Science 28*, 276-290.

Gupta, A. K., Sarkar, S., De, S., Clemens, S. C. & Velu, A. 2010: Mid-Brunhes strengthening of the Indian Ocean Dipole caused increased equatorial East African and decreased Australasian rainfall. *Geophysical Research Letters 37*, L06706, doi:10.1029/2009GL042225.

Gupta, S. M. 1988: Radiolarian zonation and volcanic ash-layers in two sediment cores from the Central Indian Basin. *Journal of Palaeontological Society of India 33*, 59-71.

Gupta, S. M. 1996: Quantitative radiolarian assemblages in the surface sediments from the central Indian Ocean and their paleomonsoonal significances. *Journal of Geological Society of India 47*, 339-354.

Gupta, S. M. 2002: Pyloniid stratigraphy-A new tool to date tropical radiolarian ooze from the central tropical Indian Ocean. *Marine Geology 184*, 85-93.

Gupta, S. M. 2003: Orbital frequencies in radiolarian assemblages of the central Indian Ocean: implications on the Indian summer monsoon. *Palaeogeography, Palaeoclimatology, Palaeoecology 97*, 97-112.

Gupta, S. M. 2009: Radiolarian abundance - a monsoon proxy responding to the Earth's orbital forcing: Inferences on the mid-Brunhes climate shift. *Earth Science India 2*, 1-20.

Gupta, S. M. & Fernandes, A. A. 1997: Quaternary radiolarian faunal changes in the tropical Indian Ocean: Inferences to paleomonsoonal oscillation of the 10°S hydrographic front. *Current Science 72*, 965-972.

Gupta, S. M., Fernandes, A. A. & Mohan, R. 1996: Tropical sea surface temperatures and the Earth's eccentricity cycles. *Geophysical Research Letters 23*, 3159-3162.

Jansen, J. H. F., Kuijpers, A. & Troelstra, S. R. 1986: A Mid Brunhes climatic event: long term changes in global atmosphere and ocean circulation. *Science 232*, 619-622.

Johnson, D. A. & Nigrini, C. 1982: Radiolarian biogeography in surface sediments of the Eastern Indian Ocean. *Marine Micropaleontology 7*, 237-287.

Johnson, D. A., Schneider, D. A., Nigrini, C., Caulet, J. P. & Kent, D. V. 1989: Pliocene- Pleistocene radiolarian events and magneto-stratigraphic calibrations for the tropical Indian Ocean. *Marine Micropaleontology 14*, 33-66.

Jones, G. A. & Johnson, D. A. 1984: Displaced Antarctic diatoms in Vema channel sediments: late Pleistocene/Holocene fluctuations in AABW flow. *Marine Geology, 58*, 165-186.

Kawamura, H., Holbourn, A. & Kuhnt, W. 2006: Climate variability and land ocean interactions in the Indo Pacific Warm Pool: A 460 ka palynological and organic geochemical record from the Timor Sea. *Marine Micropaleontology 59*, 1-14.

Kennett, J. P. & Srinivasan, M. S. 1983: *Neogene planktonic foraminefera, a phylogenetic atlas,* 265p, Hutchinson Ross, Stroudsburg.

Kershaw, A. P., Moss, P. T. & Wild, R. 2005: Patterns and causes of vegetation change in the Australian wet tropics region over the last 10 million years. *In* Bermingham, E., Dick, C.W. & Moritz, C. (eds.): *Tropical Rainforests: Past and Future,* 375-400. University Chicago Press, Chicago.

Kleijne, A. 1993: Morphology, taxonomy and distribution of extant coccolithophorids (calcareous nannoplankton). *Ph.D. thesis, Amsterdam Free University,* 321p.

Kolla, V. & Biscaye, P. E. 1973: Clay mineralogy and sedimentation in the eastern Indian Ocean. *Deep Sea Research 20*, 727-738.

Kolla, V., Bè, A. W. H. & Biscaye, P. E. 1976: Calcium Carbonate Distribution in the Surface Sediments of the Indian Ocean. *Journal of Geophysical Research 81*, 2605-2616.

Krishnaswami, S. & Sarin, M. M. 1976: Procedures for simultaneous determination of Th, Pu and Ra isotopes, Pb-210, Fe-55, Si-32 and C-14 in marine suspended phases. *Analytica Chimica Acta 83*, 143-156.

LaMontagne, R.W., Murray, R.W., Wei, K.-Y., Leinen, M. & Wang, C.-W. 1996: Decoupling of carbonate preservation, carbonate concentration, and biogenic accumulation: A 400 k. y. record from the central equatorial Pacific Ocean. *Paleoceanography 11*, 553-562.

Lisitzin, A. P. 1996: *Oceanic sedimentation, lithology and geochemistry*. 400 pp. American Geophysical Union, Washington D.C.

Mascarenhas-Pereira, M. B. L., Nath, B. N., Borole, D. V. & Gupta, S. M. 2006: Nature, source and composition of volcanic ash in sediments from a fracture zone trace of Rodriguez Triple Junction in the Central Indian Basin. *Marine Geology 229*, 79-90.

McTainsh, G. H. 1989: Quaternary Aeolian dust processes and sediments in the Australian region. *Quaternary Science Reviews 8*, 235-253

Murray, R.W., Knowlton, C., Leinen, M., Mix, A.C. & Polsky, C. H. 2000: Export production and carbonate dissolution in the central equatorial Pacific Ocean over the past I Myr. *Paleoceanography 15*, 570-592.

Nath, B. N. & Mudholkar, A. V. 1989: Early diagenetic processes affecting nutrients in the pore waters of the Central Indian Ocean cores. *Marine Geology 86*, 57-66.

Nath, B. N., Borole, D. V., Aldahan, A., Patil, S. K., Mascarenhas-Pereira, M. B. L., Possnert, G., Ericsson, T., Ramaswamy, V. & Gupta, S. M. 2008: ^{210}Pb, ^{230}Th, and ^{10}Be in Central Indian Basin seamount sediments: Signatures of degassing and hydrothermal alteration of recent origin. *Geophysical Research Letters 35,* L09603. doi:10.1029/2008GL033849.

Pattan, J. N., Gupta, S. M., Mudholkar, A. V. & Partibhan, G. 1992: Biogenic silica in space and time in sediments of central Indian Ocean. *Indian Journal of Marine Sciences 21*, 116-120.

Pattan, J. N., Masuzawa, T., Borole, D. V., Parthiban, G., Jauhari, P. & Yamamoto, M. 2005: Biological productivity, terrigenous influence and non crustal elements supply to the Central Indian Ocean Basin: Paleoceanography during the past approx. 1 Ma. *Journal of Earth System Science 114*, 63-74.

Ramaswamy, V. & Rao, P. S. 2006: Grain size analysis of sediments from the northern Andaman Sea: Comparison of laser diffraction and sieve-pipette techniques. *Journal of Coastal Research 22*, 1000-1009.

Ramesh Babu, V., Suryanarayana, A. & Murty, V. S. N. 2001: Thermohaline circulation in the Central Indian Basin (CIB) during austral summer and winter periods of 1997. *Deep-Sea Research II 48*, 3327-3342.

Sexton, P.F. & Barkar, S. 2012: Onset of Pacific-style deep-sea sedimentary carbonate cycles at the mid-Pleistocene transition. *Earth & Planetary Science Letters 321,* 81-94

Snoeckx, H. & Rea, D. K. 1994: Dry bulk density and $CaCO_3$ relationships in upper Quaternary sediments of the eastern equatorial Pacific. *Marine Geology 120,* 327-333.

Tchernia, P. 1980: *Descriptive Regional Oceanography*. 253p, Pergamon, New York.

Thierstein, H. R., Geitzenauer, K., Molfino, B. & Shackleton, N. J. 1977: Global synchroneity of late Quaternary coccolith datums: validation by oxygen isotopes. *Geology 5,* 400-404.

Thunell, R. C. & Honjo, S. 1981: Calcite dissolution and the modification of planktonic foraminiferal assemblages. *Marine Micropaleontology 6*, 169-182.

Wang, P. X., Tian, J., Cheng, X. R., Liu, C. L. & Xu, J. 2004: Major Pleistocene stages in a carbon perspective: the South China Sea record and its global comparison. *Paleoceanography 19*, PA4005, doi:10.1029/2003PA000991.

Warren, B. A. 1982: The deep water of the Central Indian Basin. *Journal of Marine Research 40*, 823-860.

Weninger, B., Jöris, O. & Danzeglocke, U. 2007: CalPal-2007 *Cologne Radiocarbon Calibration & Palaeoclimate Research Package.* http://www.calpal.de.

Winter, A., Jordan, R. W. & Roth, P. H. 1994: Biogeography of living coccolithophores in oceanic waters. *In* Winter, A. & Siesser, W. G. (eds.): *Coccolithophores,* 161-177. Cambridge University Press, Cambridge.

Wu, G., Yasuda, M .K. & Berger, W. H. 1991: Late Pleistocene carbonate stratigraphy on Ontong-Java Plateau: effects of winnowing and dissolution. *Marine Geology 96*, 193-209.

Table 1. Ranking of planktic foraminifera species in order of decreasing susceptibility to dissolution in column (a) and (b), planktic foraminifera abundance increasing order in column (c) to (f) in core BC 37 and SVBC 37

		BC 37 (W.D. 4252 m)		SVBC 37 (W.D. 3990 m)	
(a) Rank	(b) Species name	(c) Species name	(d) Average %	(e) Species	(f) Average %
1	*GIobigerinoides ruber*	*G. menardii*	62.64	*G. menardii*	25.70
2	*Orbulina universa*	*P. obliquiloculata*	8.01	*G. ruber*	13.60
3	*Globigerinella siphonifera*	*N. dutertrei*	6.60	*G. sacculifer*	12.07
4	*Globigerina rubescens*	*G. sacculifer*	5.70	*N. dutertrei*	9.64
5	*Globigerinoides sacculifer*	*G. tumida*	3.02	*P. obliquiloculata*	8.51
6	*Globigerinella aequilateralis*	*G. inflata*	2.75	*G. tumida*	5.90
7	*Globigerinoides tenellus*	*G. conglobatus*	2.74	*G. conglobatus*	5.45
8	*GIobigerinoides conglobatus*	*G. ruber*	1.80	*G. aequilateralis*	3.77
9	*Globigerina bulloides*	*G. aequilateralis*	1.72	*G. truncatulinoides*	3.47
10	*Globigerinoides quadrilobatus*	*G. truncatulinoides*	1.63	*G. bulloides*	2.42
11	*Globigerinita glutinata*	*S. dehiscens*	0.64	*G. glutinata*	1.96
12	*Candeina nitida*	*G. crassaformis*	0.62	*S. dehiscens*	1.84
13	*Globorotalia theyeri*	*G. quadrilobatus*	0.60	*G. inflata*	1.69
14	*Globorotalia truncatulinoides*	*G. bulloides*	0.39	*N. pachyderma*	1.50
15	*Globigerina inflata*	*O. universa*	0.36	*O. universa*	1.26
16	*GIoborotalia menardii*	*G. hexagonus*	0.33	*G. crassaformis*	0.45
17	*Neogloboquadrina dutertrei*	*N. pachyderma*	0.13	*G. theyeri*	0.21
18	*Neogloboquadrina pachyderma*	*G. glutinata*	0.08	*G. tenellus*	0.19
19	*Pulleniatina obliquiloculata*	*G. tenellus*	0.08	*G. rubescens*	0.15
20	*Globorotalia crassaformis*	*G. rubescens*	0.07	*G. hexagonus*	0.13
21	*Sphaeroidinella dehiscens*	*G. siphonifera*	0.04	*G. siphonifera*	0.04
22	*Globorotalia tumida*	*G. theyeri*	0.02	*C. nitida*	0.02
		C. nitida	0.02	*G. quadrilobatus*	0.02

Table 2. Chronology of core BC 37 based on biostratigraphy, radiochemical and oxygen isotope tuning (Ages are in ka)

A = Absent; P = Present; FAD = first appearance datum; LAD = last appearance datum.

Depth (cm)	*E. huxleyi*	*C. invaginata*	*S. universus*	*C. tuberosa*	Age (*E. huxleyi* based)[1]	Age (Radiolarian based)	Age ^{230}Th method	^{14}C (calibrated)	Oxygen Isotope boundaries
0-2	P	P	A	P	14.11		16.13	13.82 ± 163	
2-4	P	P	A	P	42		48		
4-6	P	P	A	P	70	<180	80		MIS 4/5, 75 ka
FAD of *C. invaginata* 180 ka				P					
6-8	P	A	A	P	98	>180	112		
8-10	P	A	A	P	126	215	145		MIS 5/6, 130 ka
10-12	P	A	A	P	155	232	177		
12-14	P	A	A	P	183	250	209		
14-16	P	A	A	P	211	267	241		
16-18	P	A	A	P	239	285	274		
18-20	P	A	A	P	268	302	306		
FAD of *E. huxleyi* 268 ka									
20-22	A	A	A	P	296	320	338	>45	
22-24	A	A	A	P	324	337	370		
24-26	A	A	A	P	352	355	403		MIS 10/11, 362 ka
26-28	A	A	A	P	380	372	435		
28-30	A	A	A	P	409	390	467		MIS 11/12, 422 ka
30-32	A	A	A	P	437	407	500		
32-34	A	A	A	P	465	<425	532		
LAD of *S. universus* 425 ka									
34-36	A	A	P	P	493	>425	564		
36-38	A	A	P	P	521		596		
38-40	A	A	P	P	550		629	>45	

[1]Considering that sediment deposition of 20 cm has taken 268 ka (FAD of *E. huxleyi*).

Table 3. Chronology of core SVBC 37 mainly based on biostratigraphy and AMS ^{14}C dates (Ages are in ka). A = Absent; P = Present; FAD = first appearance datum; LAD = last appearance datum.

Depth (cm)	*E. huxleyi*	*C. invaginata*	*S. universus*	Age (*E. huxleyi* based)	Age (Radiolarian based)	^{14}C (calibrated)
0-1	P	P	A	7.24	15	12.83±86
1-2	P	P	A	22	45	
2-3	P	P	A	36	75	>45
3-4	P	P	A	51	105	
4-5	P	P	A	65	135	
5-6	P	P	A	80	<180	
FAD of *C. invaginata* 180 ka						
6-7	P	A	A	94	188	
7-8	P	A	A	109	204	
8-9	P	A	A	123	221	
9-10	P	A	A	138	237	
10-11	P	A	A	152	253	
11-12	P	A	A	167	270	
12-13	P	A	A	181	286	
13-14	P	A	A	196	302	
14-15				210	319	
15-16	P	A	A	225	335	
16-17	P	A	A	239	351	
17-18	P	A	A	254	368	
18-19	P	A	A	268	384	
FAD of *E. huxleyi* 268 ka						
19-20	A	A	A	282	400	
20-21	A	A	A	297	<425	
LAD of *S. universus* 425 ka						
21-22	A	A	P	311	>425	
22-23	A	A	P	326		
23-24	A	A	P	340		
24-25	A	A	P	355		

Table 4. Organic carbon, $CaCO_3$ data for core BC 37 and SVBC 37. Oxygen and carbon isotope data for core BC 37

Core SVBC-37				Core BC-37					
Depth (cm)	Age (ka)	TOC %	$CaCO_3$%	Depth (cm)	Age (ka)	$\delta^{18}O$ ‰	$\delta^{13}C$ ‰	$CaCO_3$%	TOC %
0-1	13	0.21	83.40	0-2	14	-0.96	0.71	71.80	0.09
1-2	22	0.16	89.12	2-4	42	-0.09	0.75	71.80	0.09
2-3	36	0.18	86.13	4-6	70	-1.18	1.12	74.20	0.12
3-4	51	0.12	87.68	6-8	98	-0.87	1.59	75.80	0.09
4-5	65	0.16	88.19	8-10	126	-1.36	1.08	75.20	0.07
5-6	80	0.16	89.39	10-12	155	-0.93	1.28	67.80	0.05
6-7	94	0.14	88.22	12-14	183	-0.95	1.29	73.70	0.07
7-8	109	0.14	90.29	14-16	211	-0.56	0.33	72.00	0.00
8-9	123	0.14	90.58	16-18	239	-0.93	0.14	71.30	0.09
9-10	138	0.07	92.24	18-20	268	-	-	56.60	0.00
10-11	152	0.12	89.12	20-22	296	-0.29	-0.17	59.30	0.05
11-12	167	0.09	88.81	22-24	324	-0.79	-0.69	58.70	0.02
12-13	181	0.07	84.60	24-26	352	-0.50	-0.90	57.90	0.00
13-14	196	0.09	82.39	26-28	380	-1.13	0.94	52.00	0.00
14-15	210	0.07	84.10	28-30	409	-0.31	-0.41	50.20	0.00
15-16	225	0.12	80.11	30-32	437	-0.68	-0.63	48.20	0.00
16-17	239	0.07	83.48	32-34	465	-0.70	-0.46	51.10	0.00
17-18	254	0.07	84.50	34-36	493	-0.74	-0.83	51.70	0.00
18-19	268	0.05	81.30	36-38	521	-0.32	-0.36	54.40	0.00
19-20	282	0.07	78.58	38-40	550	-0.41	-0.40	55.10	0.00
20-21	297	0.02	77.61						
21-22	311	0.02	78.88						
22-23	326	0.02	79.47						
23-24	340	0.02	77.09						
24-25	355	0.00	79.21						

Figure captions

Fig. 1. Location map of seamount cores BC 37 and SVBC 37, relative percentage of kaolinite in <1 μm clay size fraction in sediments of Indian Ocean and surrounding seas (Griffin *et al*. 1968; Fagel 2007). Continental source of kaolinite for marine sediments is also shown. Arrows depict jet stream transport pathways in the Asian subcontinent while tropospheric transport path is shown from Australian continent to central Indian Basin and between Arabia and Africa (Lisitzin 1996). Locations of cores considered for discussion are shown. AAS 2/3 ($7^{o}48'$S, 80^{o}E; Gupta 2009); 716A represents ODP Hole 716A located in equatorial Indian Ocean ($4^{o}56'$N, $73^{o}17'$E); and 728B represents ODP Hole 728B in NW Arabian Sea ($17^{o}40.790'$N, $57^{o}49.553'$E) (Gupta *et al.* 2010).

Fig. 2. Detailed multibeam bathymetry of Central Indian Ocean with core locations BC 37 and SVBC 37. Left panel shows the larger view of the study area with Indian Ocean Ridge system, Rodriguez Triple Junction, fracture zones and all the dots denote the seamounts. Arrows represent the entry of AABW currents into CIB through deep saddles (5 and 10°S) of 90°E Ridge System and their movement (adopted from Gordon *et al*. 2002). Right panel shows the influence of Indian Ocean Dipole (IOD) positive and negative phases (source: www2.ucar.edu).

Fig. 3. Biostratigraphy, sedimentation rates and core description. A. Various biostratigraphic and AMS ^{14}C datum levels as a function of depth and age (BC 37). B. biostratigraphic zones and AMS ^{14}C datum of core SVBC 37. C. $^{230}Th_{excess}$ profile in core BC 37 showing average sedimentation rate of 0.62 mm ka^{-1}.

Fig. 4. Records of productivity during Mid-Brunhes Epoch. A. Oxygen isotope of *Globigerinoides ruber* of core BC 37 (long dashed curves are shown in order to emphasis low resolution data as a result of very low sedimentation rate). B. $\delta^{13}C$ of core BC 37. C. Organic carbon content (BC 37). D. $CaCO_3$ content (BC 37). E. Mass accumulation rate (MAR) of $CaCO_3$ (BC 37). F. $CaCO_3$ content of core SVBC 37. G. MAR of $CaCO_3$ (SVBC 37). H. Organic carbon content (SVBC 37). I. Total benthic foraminifera in SVBC 37 (in no. g^{-1}). J. Total planktic foraminifera in SVBC 37(in no. g^{-1}). Arrows mark events of increased productivity during the Mid-Brunhes epoch. MIS refers to Marine Isotope Stages and the numbers indicate glacial (even) and interglacial (odd) stages.

Fig. 5. Records for the Mid-Brunhes productivity and wind regime. A. Kaolinite%+chlorite% content of core BC 37. B. Sediment size class 8-16 μm. C. Sediment size class < 2 μm. D. Percent distribution of *Globigerina bulloides* and E. Percent of *Cymbaloporetta squammosa* showing a decrease at ~300 ka at Hole 716 A (data of Gupta *et al.* 2010). F. *G. bulloides* percent at Hole 723B

(NW Arabian Sea) (Emeis *et al.* 1995) showing a intensification of SW monsoon from ~300 ka onwards. G. Spore/pollen ratio (Kawamura *et al*. 2006) showing a decrease at ~300-250 ka indicating vegetation changes. H. Radiolarian/gram at Central Indian Ocean (Gupta 2009) showing an increase at about ~250 ka. I. Insolation (30°N-30°S May-July). J. ETP (MIS = marine isotope stages, MIS and numbers are the same as in Fig. 4).

Fig. 6. Coccolithophores records from CIB demonstrate the dominance of the Gephyrocapsa spp. and reduction in Shannon-Wiener Diversity index during the Mid-Brunhes interval. A. *Gephyrocapsa Oceanica* %. B. *Gephyrocapsa Caribbeanica* %. C. *Gephyrocapsa* spp. D. Shannon-Wiener Diversity index (H'). E. *Emiliania huxleyi* % (FAD of *B. Invaginata*, *E. huxleyi* and LAD of *S. universus* are marked with arrows). Global Mid-Brunhes dissolution interval (MBDI) is marked by a striped gray box (MIS = marine isotope stages).

Fig. 7. Mid-Brunhes Dissolution Interval and carbonate dissolution proxies of core BC 37. A. *Neogloboquadrina dutertrei.* B. *Pulleniatina obliquiloculata*. C. Total resistant species. D. *Globorotalia menardii.* E. *Globigerinoides ruber* (dissolution susceptible species). F. *Globigerinoides bulloides* (dissolution susceptible species). G. $CaCO_3$%. H. Dissolution index (ratio of non-resistant species to resistant species). I. Insolation (30°N-30°S May-July). J. ETP.

Fig. 8. Carbonate dissolution proxies of core SVBC 37. A. *Globorotalia menardii* %. B. *G. menardii* fragments. C. Resistant species %. D. *Pulleniatina obliquiloculata* %. E. *Neogloboquadrina dutertrei* %. F. *Globigerinoides ruber* %. G. *Globigerina bulloides %*. H. $CaCO_3$%. I. Dissolution index (ratio of non-resistant to resistant species).

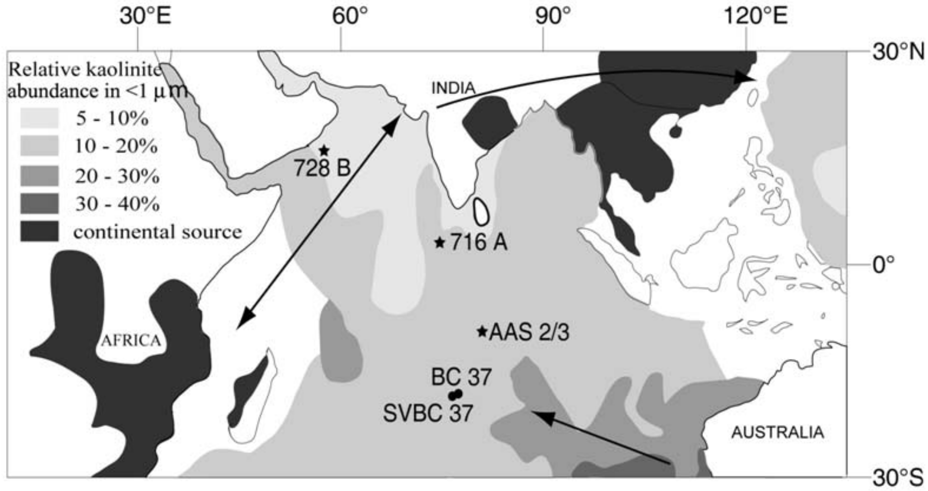
30°E
60°
90°
120°E
30°N
0°
30°S
Relative kaolinite abundance in <1 µm
5 - 10%
10 - 20%
20 - 30%
30 - 40%
continental source
INDIA
728 B
716 A
AFRICA
AAS 2/3
BC 37
SVBC 37
AUSTRALIA

Fig. 1

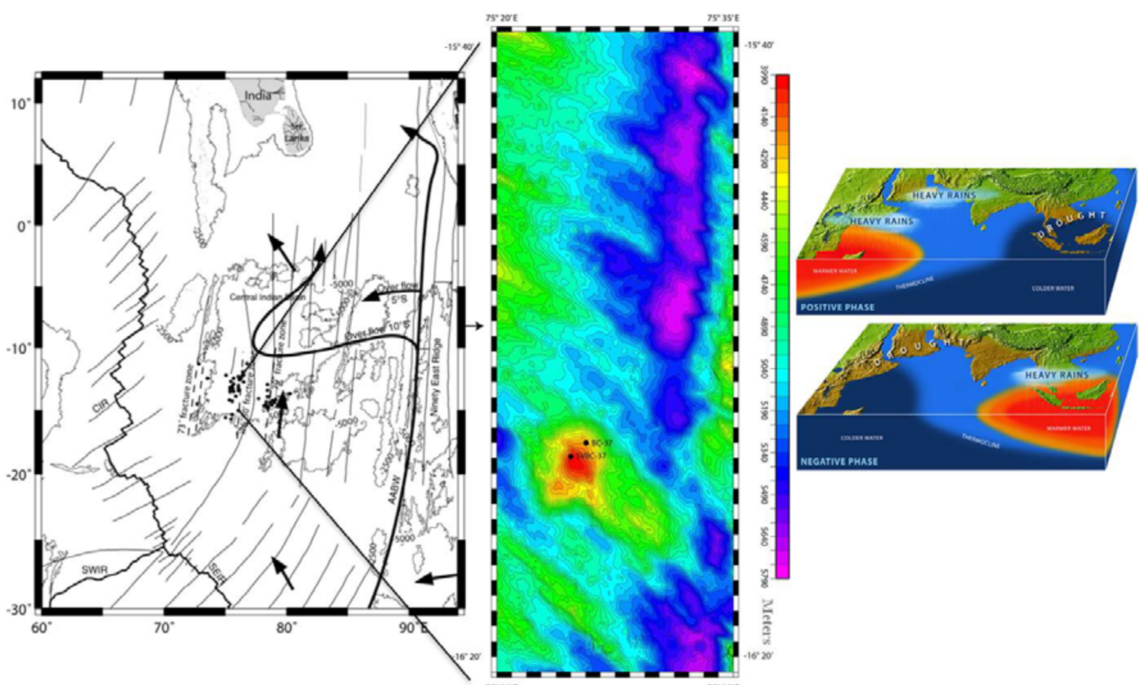
10°
0°
-10°
-20°
-30°
60°
70°
80°
90°E
India
Central Indian Basin
Ninety East Ridge
AABW
CIR
SWIR
SEIR
75° 20'E
75° 35'E
-15° 40'
-16° 20'
BC-37
SVBC-37
Meters
HEAVY RAINS
DROUGHT
WARMER WATER
THERMOCLINE
COLDER WATER
POSITIVE PHASE
NEGATIVE PHASE

Fig. 2

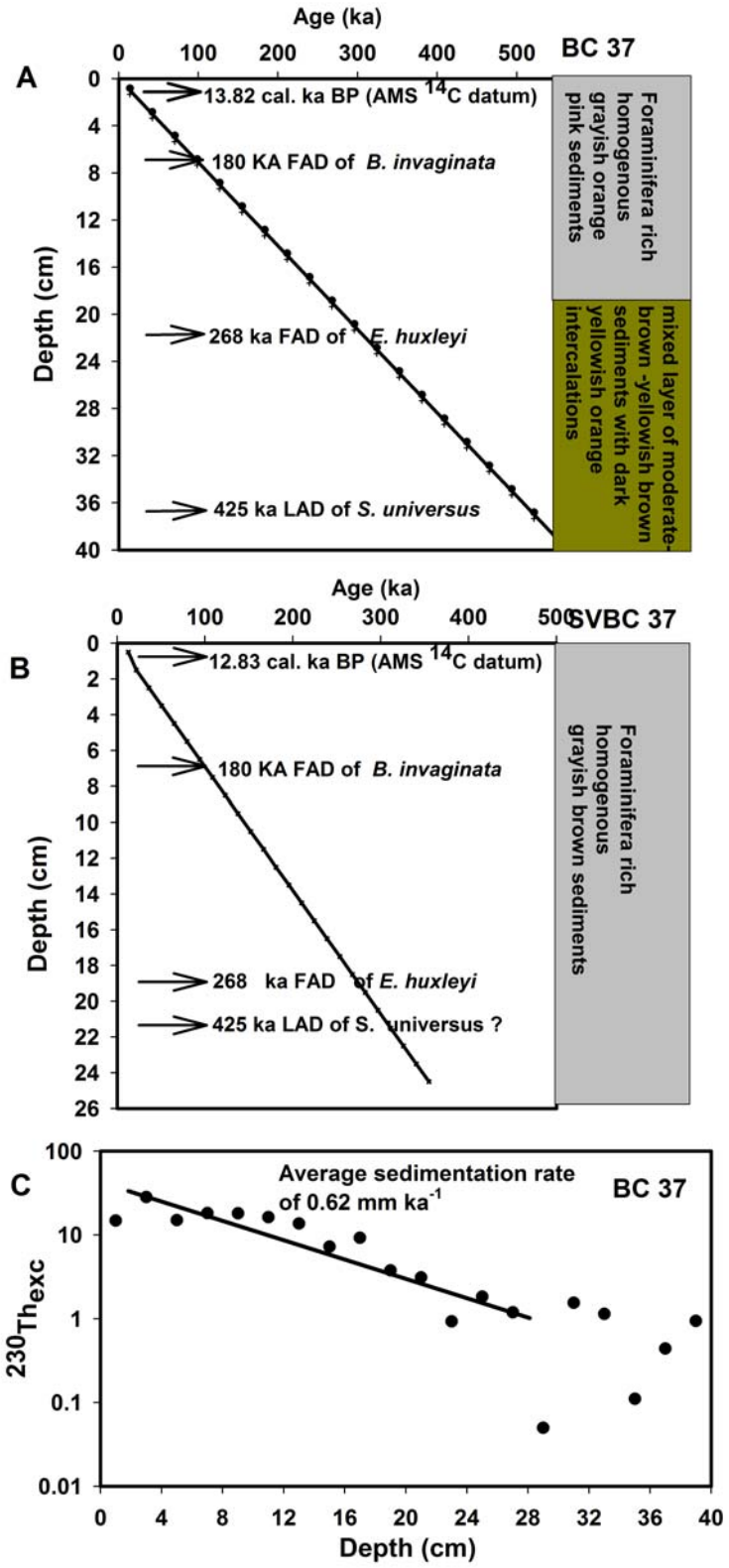
A
Age (ka)
0 100 200 300 400 500
BC 37
13.82 cal. ka BP (AMS 14C datum)
180 KA FAD of B. invaginata
268 ka FAD of E. huxleyi
425 ka LAD of S. universus
Depth (cm)
0 4 8 12 16 20 24 28 32 36 40
Foraminifera rich homogenous grayish orange pink sediments
mixed layer of moderate-brown -yellowish brown sediments with dark yellowish orange intercalations
B
Age (ka)
0 100 200 300 400 500
SVBC 37
12.83 cal. ka BP (AMS 14C datum)
180 KA FAD of B. invaginata
268 ka FAD of E. huxleyi
425 ka LAD of S. universus ?
Depth (cm)
0 2 4 6 8 10 12 14 16 18 20 22 24 26
Foraminifera rich homogenous grayish brown sediments
C
Average sedimentation rate of 0.62 mm ka-1
BC 37
230Thexc
100 10 1 0.1 0.01
0 4 8 12 16 20 24 28 32 36 40
Depth (cm)

Fig. 3

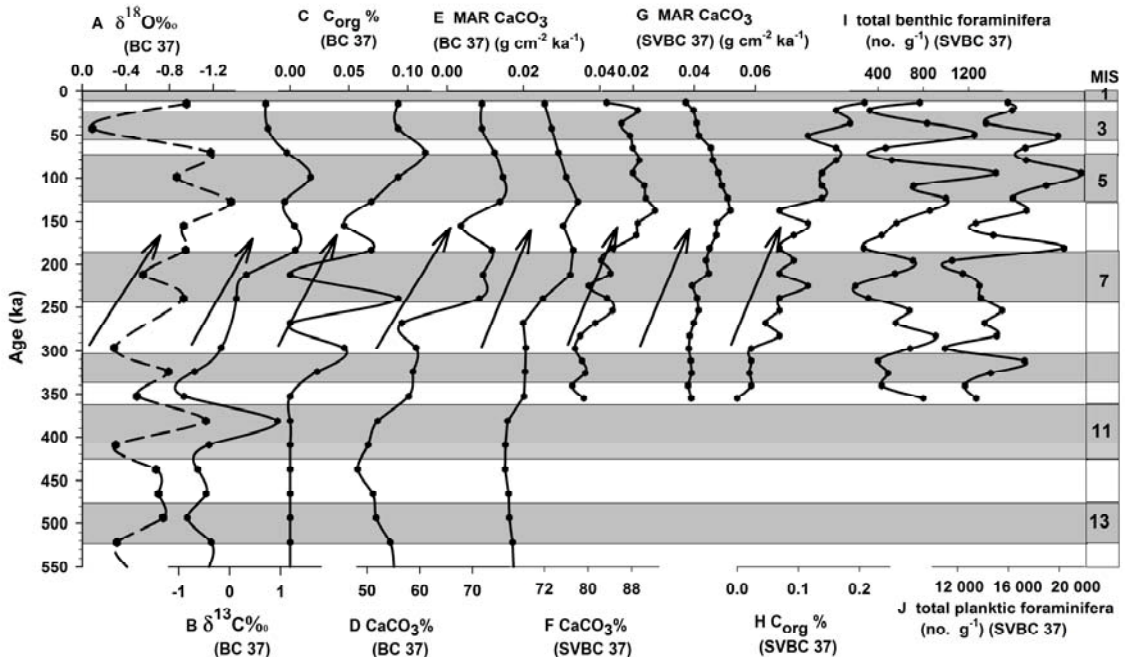
A δ18O‰ (BC 37)
C Corg % (BC 37)
E MAR CaCO3 (BC 37) (g cm-2 ka-1)
G MAR CaCO3 (SVBC 37) (g cm-2 ka-1)
I total benthic foraminifera (no. g-1) (SVBC 37)
MIS
Age (ka)
B δ13C‰ (BC 37)
D CaCO3% (BC 37)
F CaCO3% (SVBC 37)
H Corg % (SVBC 37)
J total planktic foraminifera (no. g-1) (SVBC 37)

Fig. 4

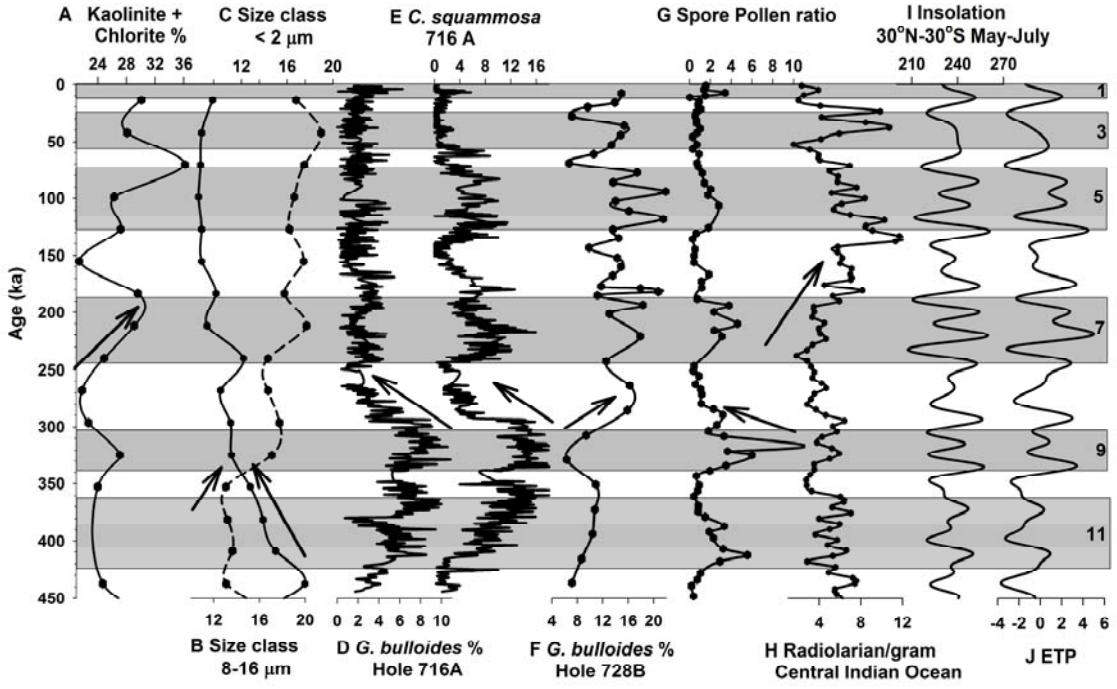
A Kaolinite + Chlorite %
C Size class < 2 μm
E C. squammosa 716 A
G Spore Pollen ratio
I Insolation 30°N-30°S May-July
Age (ka)
B Size class 8-16 μm
D G. bulloides % Hole 716A
F G. bulloides % Hole 728B
H Radiolarian/gram Central Indian Ocean
J ETP

Fig. 5

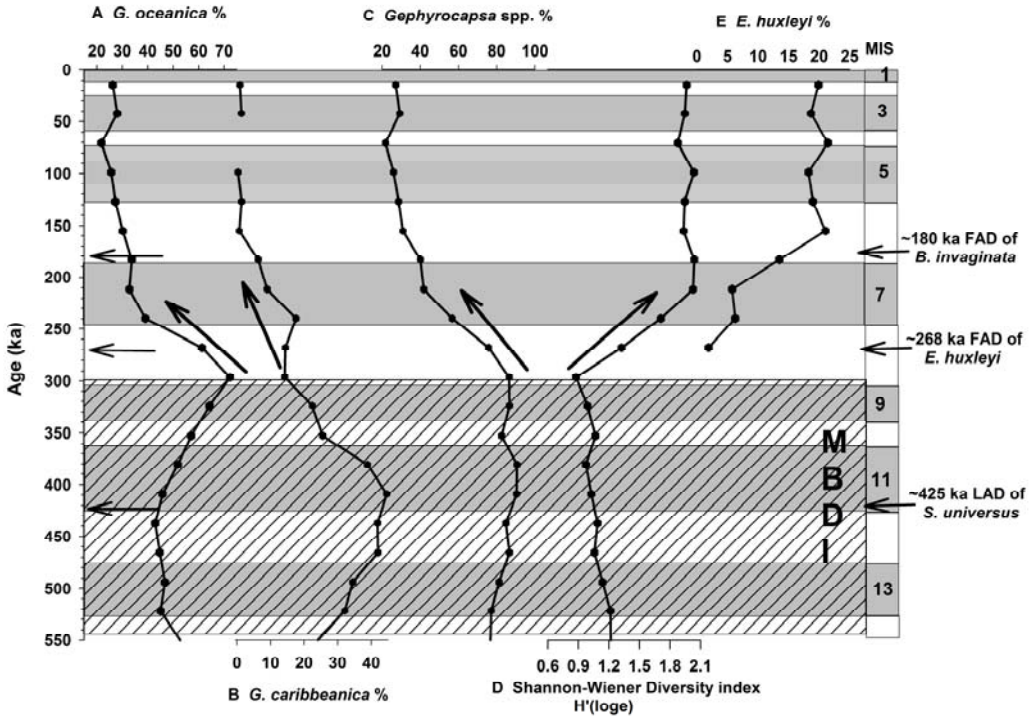
A G. oceanica %
C Gephyrocapsa spp. %
E E. huxleyi %
MIS
Age (ka)
~180 ka FAD of B. invaginata
~268 ka FAD of E. huxleyi
~425 ka LAD of S. universus
M
B
D
I
B G. caribbeanica %
D Shannon-Wiener Diversity index H'(loge)

Fig. 6

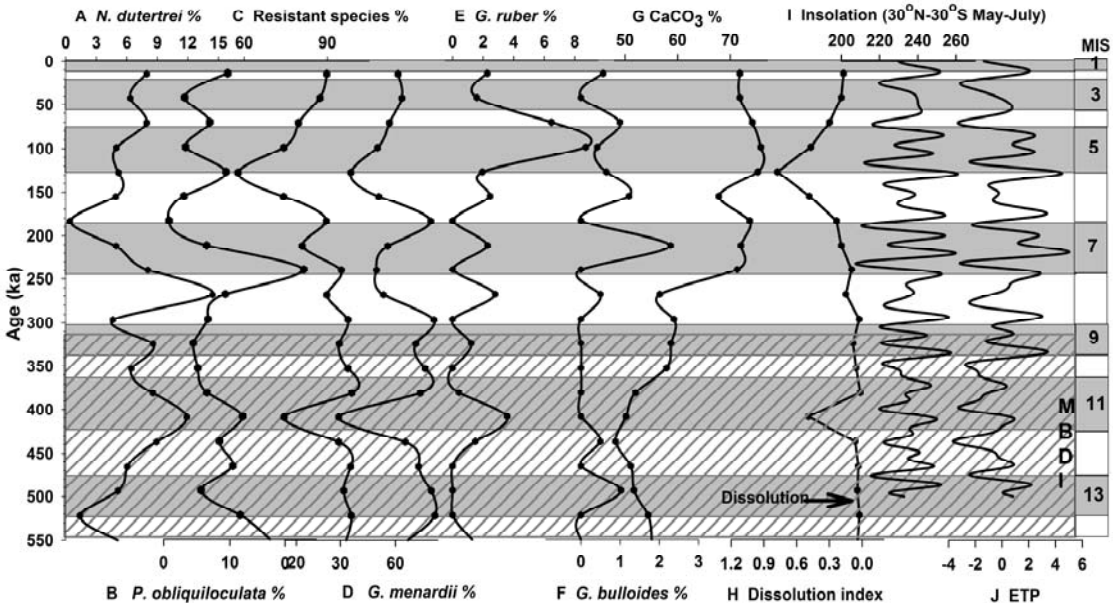
A N. dutertrei %
C Resistant species %
E G. ruber %
G CaCO3 %
I Insolation (30°N-30°S May-July)
MIS
Age (ka)
Dissolution
B P. obliquiloculata %
D G. menardii %
F G. bulloides %
H Dissolution index
J ETP

Fig. 7

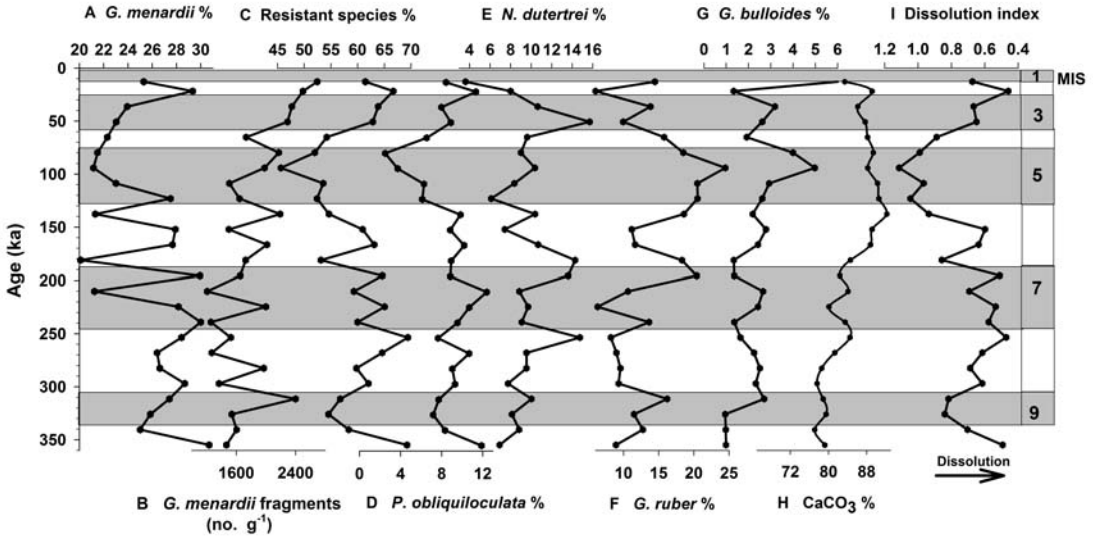
A G. menardii %
C Resistant species %
E N. dutertrei %
G G. bulloides %
I Dissolution index
MIS
Age (ka)
Dissolution
B G. menardii fragments (no. g-1)
D P. obliquiloculata %
F G. ruber %
H CaCO3 %

Fig. 8